Final report

This final report is organized according to the workplan tasks

T1.Installation of the VLF receiver at Princess Elisabeth base

The Geographical Coordinates of the base are : -71.95, 23.25, Magnetic Latitude: L=5.68
The installation was done by Fabien Darrouzet and János Lichtenberger during the trip to Antarctica between 4 January -13 February 2016.

The setup for the AWDANet station at Princess Elisabeth (PE) consists of the following parts:

1. VLF antenna: 2 search coils+line driver.
2. Waterproof box for VLF antenna
3. Protecting box for VLF antenna
4. VR2 high time precision data logger
5. Automatic Whistler Detector (AWD) and Automatic Whistler Analyzer (AWA) pre-processing PC
6. AWA PC with GPGPU cards

The equipment were packed and sent to AntartctiQ (the company manages PE with Belgian Army) to Wervik, Belgium on 14 December 2014. All cargo were carried from Cape Town to Antarctica by Antarctic Logistics Centre International (ALCI) on 8 January 2016.
All equipment excluding the sensor were planned to install in the North Science Shelter that is located ~500m north to the base. The location for the sensor was preliminary set to 500m east to North Science Shelter. To make a final decision we made test measurements on 11 and 12 January by a portable VLF search coil. The analogue signal was fed to a USB soundcard that was connected to a laptop running baudline real-time spectrum analyzer software. The signal was free of man-made noise and interference except from the 50Hz harmonics and static noises generated by the electrostatic discharges from the snow. We manufactured a wood 'table' to hold the protecting box and the SC (Figure 1). This setup was also suitable to avoid snow deposition by the snow drift.
The cable was laid down into a trench to protect again accidental mechanical damage by people or vehicles. We used A7W1-P005L-02 cable, it has 5 twisted pair wires and the cross section of a wire is 0.5 mm2. The insulation material specified for very low temperature (-40 degree) suitable for Antarctica. The cable was pulled into a 20x2.3mm hard polyethylene pipe to add further mechanical protection, mainly against slow drift of compacted snow.
We put the VR2 data logger and the two PCs into the Northern Science Shelter. However a few hours after switching on the PCs, the temperature inside went up to 35-38 degrees, though the PCs were just idling, consuming ~200W only. During normal operation, the expected max power consumption is 800-1000W, thus we realized that the shelter is not suitable for the PCs. The outside temperature was -10- -15 degrees, but the shelter is insulated very well and due to the snow drift, no open ventilation holes are allowed in the wall/door of the shelter. Therefore we moved the PCs to the main building. The measurement operated normally since the installation and collected VLF data continuously (Figure 2). Princess Elisabeth is unmanned during the southern hemisphere winter (from mid-February till end of November). During this period, the power is supplied by an autonomous power grid with battery backup. The connection to PE broke on 22 May 2016 due to a failure in the power grid synchronization. Unfortunately, the next expedition (Nov 2016 – Feb 2017) was canceled due to Belgian internal problem, while the last expedition (Nov 2017 – Feb 2018, with a new management organization) was able to do minimal recovery measures only at the base. The recent expedition, on the way to PE plans to restore the original state of the experiments and restart the normal operation.

Figure 1. The search coils and line driver on the assembly board inside the waterproof HPRC box placed into the insulated wooden box.

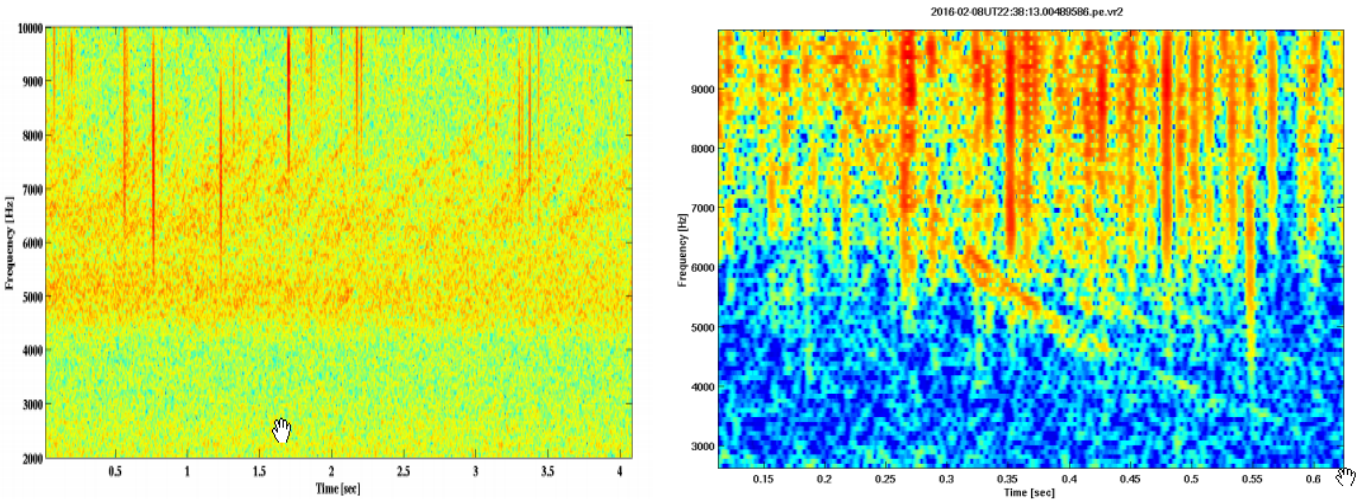

Figure 2. (left) VLF chorus emission recorded at PE, (right) whsitler recorded at PE.

T2. Development of an automatic algorithm to detect choruses in VLF signal

The AWD algorithm is able to detect whistlers in the raw VLF signal. This algorithm formed the base for the development of the automatic chorus detector. There are fundamental differences between whistlers and choruses in the frequency span, duration and the shape of the signals, but it was possible to use the basic principles of whistler detector, that is based on three steps:

1. ‘cleaning’ of the raw signal – removing the natural (sferics) and man-made (VLF transmitters, power line harmonics) signals;

2. 2D correlation with a model whistler spectrogram;
3. creating an adaptive threshold from background noise level and discriminate the 2D correlation output against the adaptive threshold [Lichtenberger et al., JGR, 2008].

In the new chorus detector algorithm we used a 'cleaning' algorithm based on an old paper [Dowden, Proc. IRE, 1963]. This analogue technique uses a partially unidirectional integrator having a long time constant for signal increases and a very short one for signal decreases. We implemented this analogue technique in digital form using 25 sec for the signal increase and 0.001sec for signal decrease. The implemented not only algorithm removes the unwanted noises but automatically sets the detector threshold to zero. The apparent disadvantage of this method is that is suppresses the weak signals as well. However we can use only those choruses for the estimation of energetic electron densities our that have high enough SNR and frequency span – these are required for the accurate determination of the frequency sweep rate and reconstruction of the chorus propagation. Test data set was selected using these conditions first by visual data inspection – the experiences gained from AWD development proved that this is the best method. Then the chorus detector was tuned on this test data set. A simulated run was performed on a two year long synoptic data set from another high magnetic latitude station (Halley, Antarctica). The overall efficacy of the detector algorithm was about ~25-28%, but it was ~80% for the those choruses that can be used to determine the frequency sweep rate and reconstruct the propagation.

T3. Analysis of energetic electron distribution measured by Cluster and RBSP spacecrafts

Energetic electrons are injected during geomagnetic storms into the inner-magnetosphere in the energy range of few keV – 100 keV, providing free energy for chorus wave generation. To better understand the process of energetic plasma diffusion from the solar wind through the Earth's foreshock to the inner magnetosphere, we have investigated the field-aligned diffusion of energetic ions by using quasi-linear theory and test particle simulation [Otsuka et al. 2018]. This theory was completed by studying the energetic ion diffusion processes using Cluster measurements [Kis et al. 2018A] and modeled by 1D hybrid simulation [Kis et al., 2018b].

Our aim was to identify isotropic pitch-angle distributions of energetic electrons and localize the energy ranges in which the interaction with whistler mode waves can be happen. The Van Allen Probe mission is ideal for detailed investigation of energetic electrons: the twin satellites are flying a slightly different, nearly equatorial (inclination 10.2◦) and highly elliptical orbit with perigee 618 km and apogee 30,414 km (5.8 RE). Both spacecrafts carry a wide range of particle detectors, in this project we use the Helium Oxygen Proton Electron (HOPE) instrument as it can produce a high quality dataset by measuring electrons and dominant ion species in the energy range of 1 eV - 50 keV in 72 logarithmically spaced steps, with a 4π sr field of view, and a fixed time cadence of ~ 24 sec. The wide field of view enable us to transform the primarily datasets of sector-energy-detector-time to the time-energy-pitch angle dependent counts product, using mode 0 only (the main science mode data). The first challenge is that the counts of energetic electrons are too low to show clear pitch angle distributions (PADs) most of the time. Moreover the 5 detector pixels, which form the HOPE instruments, are not intercalibrated, during the mission they have been aging differently resulting in dissimilar sensitivity.

To increase the reliability of PADs measured by HOPE, averaging methods have been used on Level 1 counts data: assuming a Poisson distribution of incoming particles, the signal to noise ratios (SNR) were calculated as the square root of total counts. Then the data was analyzed by using moving averages with different window lengths: the window size grows until the total count content reaches 144 (i.e SNR =12), then moves on. On the other hand the time resolution of the measurements is reduced during low count rate periods. This simple method can be a great tool to increase the accuracy

of HOPE measurements, but quite calculation expensive. A reasonable compromise is to use an average window length, which - based on our experiences - is 5 min [Juhász et al. 2017].
Besides low count rates, the different gains of pixel detectors can cause other uncertainties in pitch angle resolved data. Assuming that count rates change relatively slowly, we can use total count rates of the common pitch angle areas of neighboring detectors to compare detector gains. Selecting those time periods when the total electron count (all directions and energies above 1 keV) is higher than 200, a list of daily ratios are created referring to the middle detector. It must be noted that detector pixels of ±72° overlap ten times less, the accuracy of the ratios derived from these detectors can be higher. The calibration ratios, calculated for the entire mission, vary between 0.4-1.8 . Comparing the changes of calibration ratios to the DST and energetic particle data from MAGEIS, it is obvious that geomagnetic storms effect the performance of HOPE.

The sensitivity of HOPE data, which results in noisy pitch angle distributions due to low count rates despite of the 5 min averages, led to a robust method. We increased counting statistics by assuming PAD symmetry around PA = 90◦ and sum the counts while ignoring loss cone, then define 3 boxes in the domain of pitch angles and compute ratios (A±SNR) / (B±SNR) and (A±SNR) / (C±SNR). If both are in the range of 0.8 – 1.2, then the given PAD is declared to be isotropic (Figure 3). Comparing these time periods of isotropy with increased electron fluxes, we created a list of possible events of wave-particle interactions.

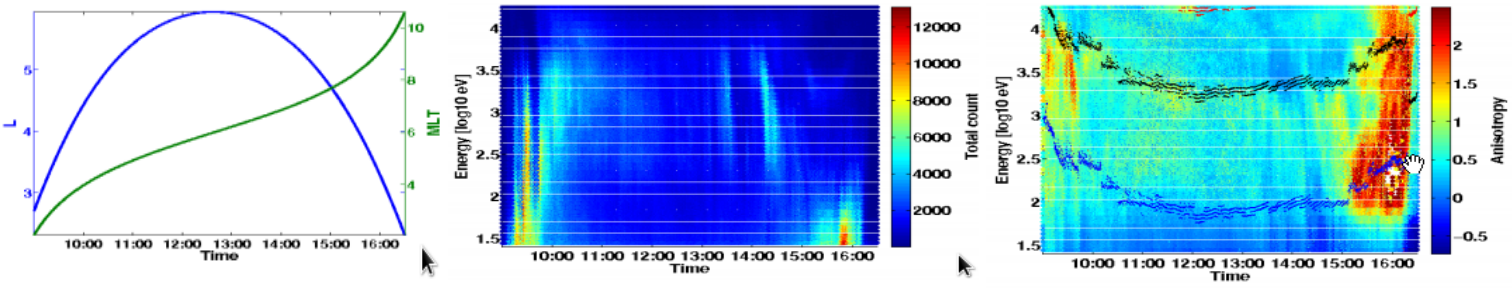

Figure3. (left panel) L and MLT value, (middle panel) Total electron count, (left panel) Anisotropy of PADs and the minimum electron energy of relativistic resonance with chorus waves of various frequencies (blue: 0.8fce, black: 0.5 fce, red: 0.2 fce) on1 4th November 2012

T4. Development of chorus-wave propagation model.

The propagation path of whistler mode chorus waves recorded on the ground is not known, therefore we have to model it and confirm the model with measurements. The reason why we need to now the propagation path is directly related to the connection of frequency sweep rate of the generated chorus elements to the optimum wave amplitude. The generation takes place at the magnetic equator, the chorus wave stat to propagate from there and undergo frequency dependent dispersion during the propagation. As a result, the frequency sweep rate measured on chorus elements recorded on the ground differ from the original one and has to be corrected to obtain the correct optimum wave amplitude. The wave propagation model consists of three sections:

1. propagation from the origin to the top of the ionosphere (magnetospheric part);
2. propagation through ionosphere;

3. propagation from the ionospheric exit point to the receive in the Earth-Ionosphere waveguide.

There was a consensus until recently that whistler mode waves observed on the ground propagate in ducts – density enhancement, depletion or sharp gradient. The evidence of ducts are still indirect [Helliwell, 1965], but recent active measurement on IMAGE satellite [Carpenter et al., 2002] exhibit evidences of field aligned density irregularities, both inside and outside of the plasmapuase.
Ground VLF transmitter signals recorded on board the Demeter and Van Allen Probes propagate mostly along the filed lines in ducted mode (Figure 4) [Koronczay et al., 2018].

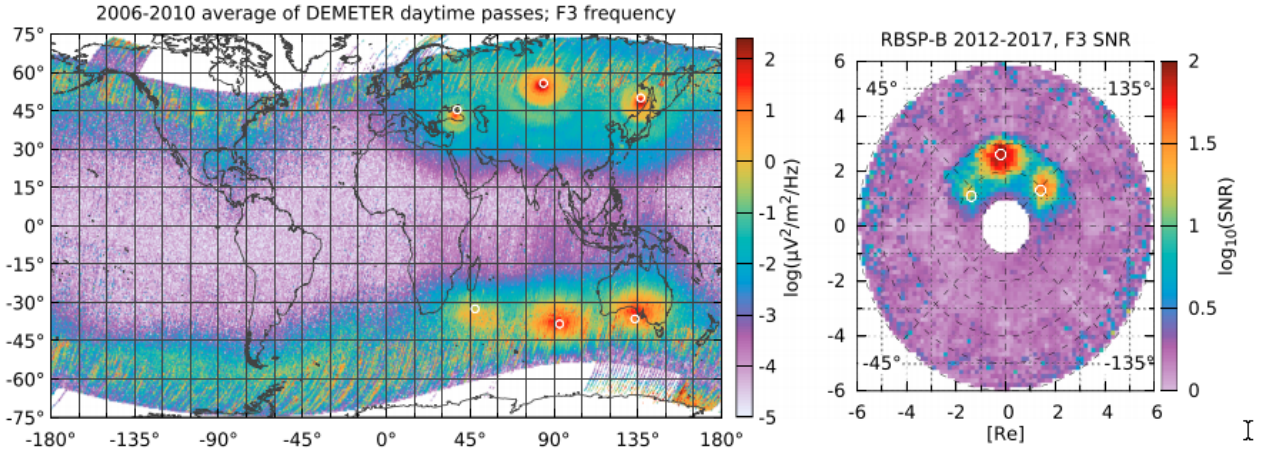

Figure 4. (left) Average electric field in the F3 alpha frequency above background levels. Long-term average based on the ICE instrument of the DEMETER satellite in low Earth orbit,White circles are the locations of the three main Alpha transmitters and their magnetic conjugates. (right) Average signal-to-noise ratio of the 14.8kHz alpha transmitter frequency in the equatorial plane, based on HFR measurements of the EMFISIS instrument onboard the RBSP-B satellite. White circles denote the intersection of the plane and the magnetic field lines starting at the transmitters.

Recent studies [Golden et. al., 2010] opened the possibility of non-ducted propagation through inverse 3D ray-tracing calculations. These calculations always led to two major conclusions: a) the wave normal angle of the wave at the origin is large, often 90 degrees; b) the plasmapause locations were within +0.6L - -0.3L range of the receiver. The conclusion a) is in direct contradiction with the latest theory of chorus generation [Omura and Nunn, 2011], as the generated waves start to propagate along the field line with wave normal parallel to the magnetic field. Thus the non-ducted propagation may be excluded from the model. Conclusion b), however in accordance with the standard ducted propagation scenario: a whistler mode wave packets can be recorded within 800-1000km radius of the ionospheric exit point.
As field aligned density irregularities outside the plasmapause are found in IMAGE measurements, thus ducted propagation outside the plasmapause cannot be excluded. However from the long history of whistlers recorded on the ground complemented our resent studies using our AWDANet observations show very low percentage of non-plasmaspheric propagation. The only feasible propagation path thus the plasmapause itself. This is in accordance with the found close vicinity of the plasmapause during ground observation (conclusion b) above) and with the theoretical considerations that the plasmapause sharp density gradient can act as a guiding structure [Helliwell, 1965] and experimental evidences of knee whistlers [Carpenter, 1963]. The chorus waves generated at the magnetic equator start to propagate along the field line with wave normal parallel to the magnetic field. However – if no density duct along the field line – the wave propagation start to deviate from the filed line quickly due to the gradient in the magnetic field and electron density. The wave propagation model used for the

magnetospheric part is the full wave solution of Maxwell's equations [Ferencz et al., 2001]. Therefore we assumed the following propagation scenario in the magnetosphere: a. the chorus waves are generated at the equator, near the plasmapause and start propagate along the field line; b. as the magnetic field and density gradient alter the wave direction, the waves diverted toward the plasmapause are trapped by the steep density gradient and guided along the plasmapause (field line) if their wave normals fall into the trapping cone.

In the ionospheric path, the standard model (horizontally layered model) is used with scattering assumption, that is at the top of the ionosphere, the power density of the ducted energy is more-or-less independent of wave normal direction in the duct due to the small irregularities in the refractive index. However the electron density of the ionosphere, more notable the F2 layer is affected by the geomagnetic disturbances that may affect the propagation [Berényi at al., 2017]

The wave energy leaks through the transmission cone to the Earth-Ionosphere waveguide. We have performed a preliminary statistic compared chorus detected at high latitude AWDANet stations (Halley and SANAE) with the location of the plasmapause and found that the difference between the plasmapause location and the recording site is <= +-1.0L that correspond to ~800km latitudinal difference at those locations. This is in agreement with the statistics performed on Palmer (Antarctica) data [Golden et al, 2010].

The magnetospheric part of developed chorus wave propagation model uses the model used in whistler inversion [Lichtenberger, 2009] and in fractional inversion of VLF transmitter signals [Koronczay et al., 2018]. In the development and validation of the chorus propagation model, we used in-situ cold electron density measurements from Van Allen Probes. The used [Denton at al., 2004] field aligned density distribution model as it is valid both for plasmasphere and plasmatrough. In the future, when we apply the model to choruses recorded on the ground and in-situ cold electron density measurements may not be available, we use the trough model of [Zhelavskaya et al., 2016] to obtain the equatorial electron density.

T5. Derivation of optimal wave amplitude from frequency sweep rate of chorus elements [Juhász et al., 2018].

The theory of the generation process of chorus emissions developed by [Omura et al.,2008] and [Omura and Nunn, 2011] concludes that the resonant electric current is a function of the inhomogeneity ratio and at the geomagnetic equator it has a maximum at S=0.41. The frequency sweep rate is proportional to the wave amplitude and the chorus generation takes place with the optimum wave amplitude. The optimum wave amplitude is proportional to the density of the energetic electrons. This is the parameter we plan to derive from a measured parameter (the frequency sweep rate). In the factor that connects the frequency sweep rate with the optimum wave amplitude, there are two unknown parameter have to be derived: the parallel and minimum perpendicular thermal velocity of the energetic electrons. The distribution function is assumed to be a bi-Maxwellian one. We estimate the actual parallel velocity for a given frequency is set to the resonance velocity and it can be calculated from the resonance conditions. To estimate the parallel and the minimum perpendicular thermal velocities, we use the relativistic linear growth-rate of R-mode plasma waves [Xiao et al., 1998]. First we identify the band of whistler-mode waves corresponding to the linear wave growth. Assuming arbitrary energetic electron density, N_h, we search for those parallel momentum $U_{t||}$ value, that produces the maximum linear growth rate at the mean frequency of the linear wave growth band. In the knowledge of $U_{t||}$, a minimum estimate for perpendicular thermal velocity $V_{\perp 0}$ can be calculated. Then, assuming non-linear wave growth, with the obtained velocities, the optimal wave amplitude can be derived (Figure 5.)

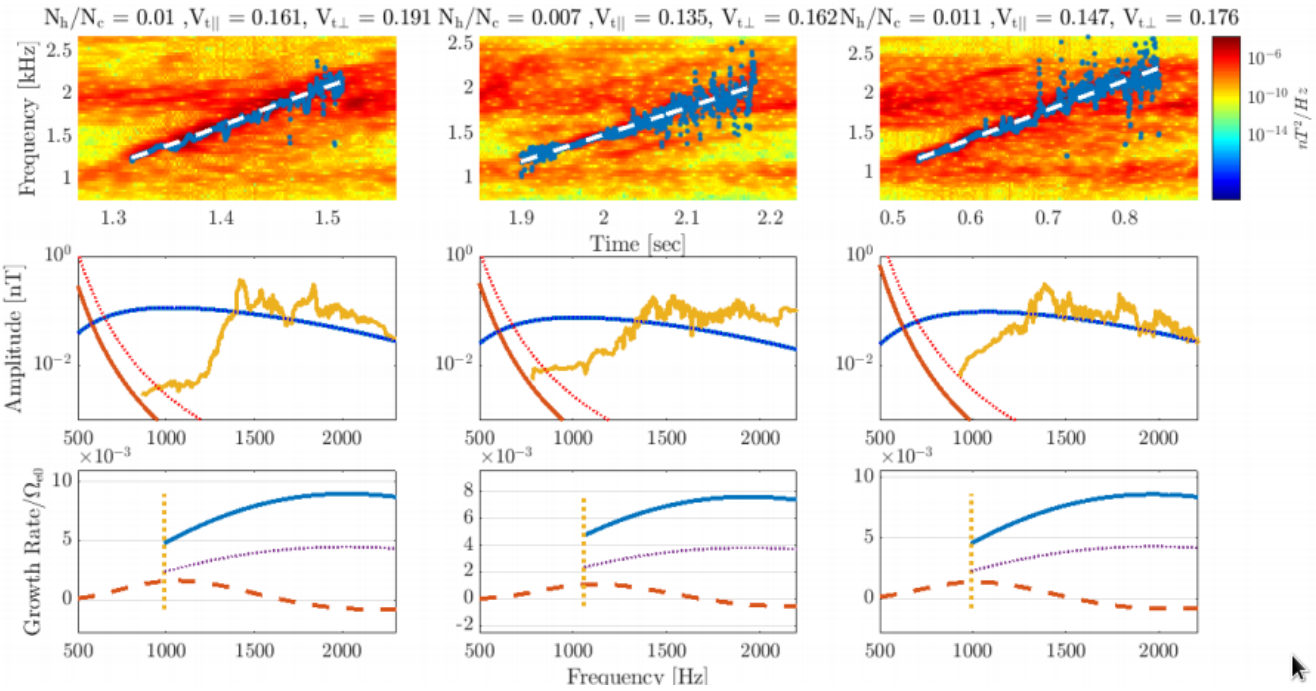

Figure 5. Chorus emissions from 2012-11-14UT11:01:17.986 (left column), 2012-11-14UT11:14:24.570 (middle column) and 2012-11-14UT11:15:59.202 (right column). In the upper row the spectrogram, instantaneous frequency (blue lines) and the linear approximation (dashed white lines) of the emissions are shown. The optimum amplitudes (middle panels, blue lines) are of the same order as the measured amplitude (yellow lines), and are not affected by the change of τ (the ratio of nonlinear transition time and nonlinear trapping period) . Threshold amplitudes of τ= 0.5 and 0.25 are plotted by solid and dotted red lines, respectively. The threshold amplitude does not depend on τ directly. However, changes of τ modify N_h/N_c, which affects the threshold amplitude. Bottom panels: linear growth rate (dashed red line), ω_{rm} (yellow dashed lines). Nonlinear wave growth rates are plotted by blue solid (τ = 0.5) and dotted (τ = 0.25) lines.

T6. Development of a semi-automatic algorithm to determine the frequency sweep rate of chorus elements.

To determine the frequency sweep rate of a chorus element, we calculate the instantaneous frequencies. In the case of spacecraft measurements the three magnetic wave components are applied. First, we transform the magnetic wave vectors to a local coordinate system where we get a parallel and two perpendicular components with respect to the Earth's magnetic field line at the spacecraft position. By identifying the zero crossings of one of the perpendicular waveform components, we can obtain a non-uniform time series of sampling. From this the instantaneous frequencies can be calculated.
In the case of ground based measurements, that usually consist of two perpendicular components (NS and EW), we can obtain the non-uniform time series of sampling using any of the components. We generally use the NS component as it is the stronger one.

The use of the zeros crossings gives us a frequency corresponding to the highest amplitude at a given time. In order to minimize the effects of noises, we applied a bandpass filter in the frequency range of the chorus element before the calculation of instantaneous frequencies. In the last step, a linear fit is made on the instantaneous frequency points to obtain the frequency sweep rate ($d\omega/dt$, Figure 7).

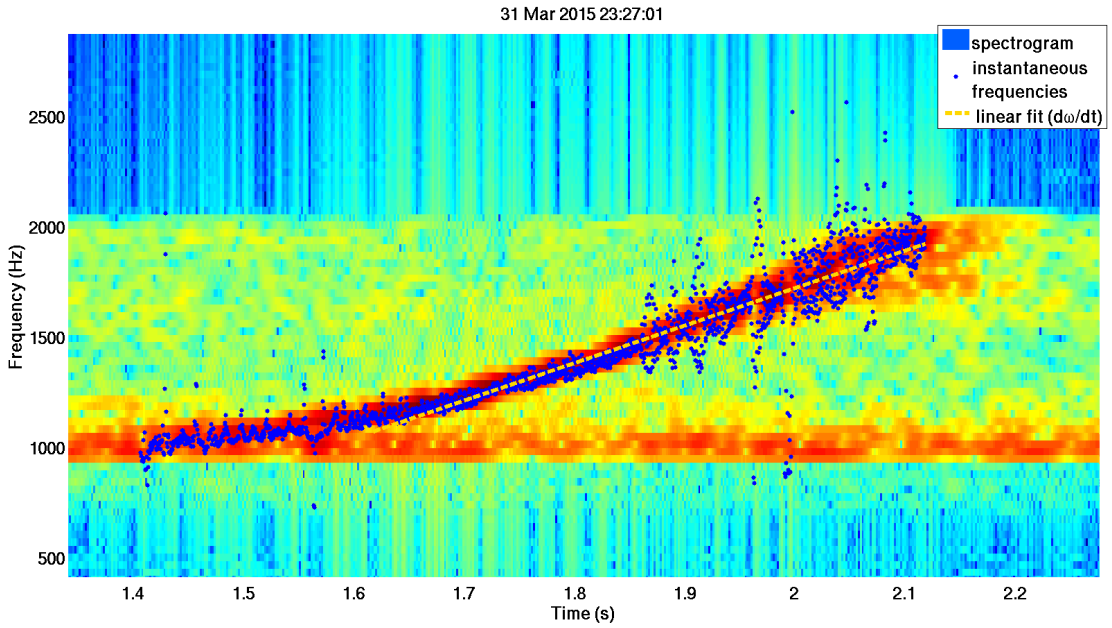

Figure 7. Illustration of the semi-automatic method developed for obtaining the frequency sweep rate from spectrogram of chorus emission applied to EMFISIS burst data.

T7. Validation of the energetic electron densities derived from choruses with in-situ measurements

The inversion method consists of two phases (Figure 6). First we estimate the parallel and minimum perpendicular thermal velocity of the source population using the relativistic solution of electromagnetic R-mode wave instability of (Xiao et al., 1998) (1st phase blue box in Fig.6). Using these thermal velocities, a direct estimation of N_h/N_c is obtained from the frequency sweep rate of a chorus emission using nonlinear wave growth theory (2nd phase, blue box). For this study, the inputs are gyrofrequency Ω_e, plasma frequency ω_{pe}, frequency sweep rate of an individual chorus emission $\partial\omega/\partial t$ and the mean frequency of the assumed band of linear growth ω_{rm}, all from EMFISIS measurements (red boxes on Fig.6).

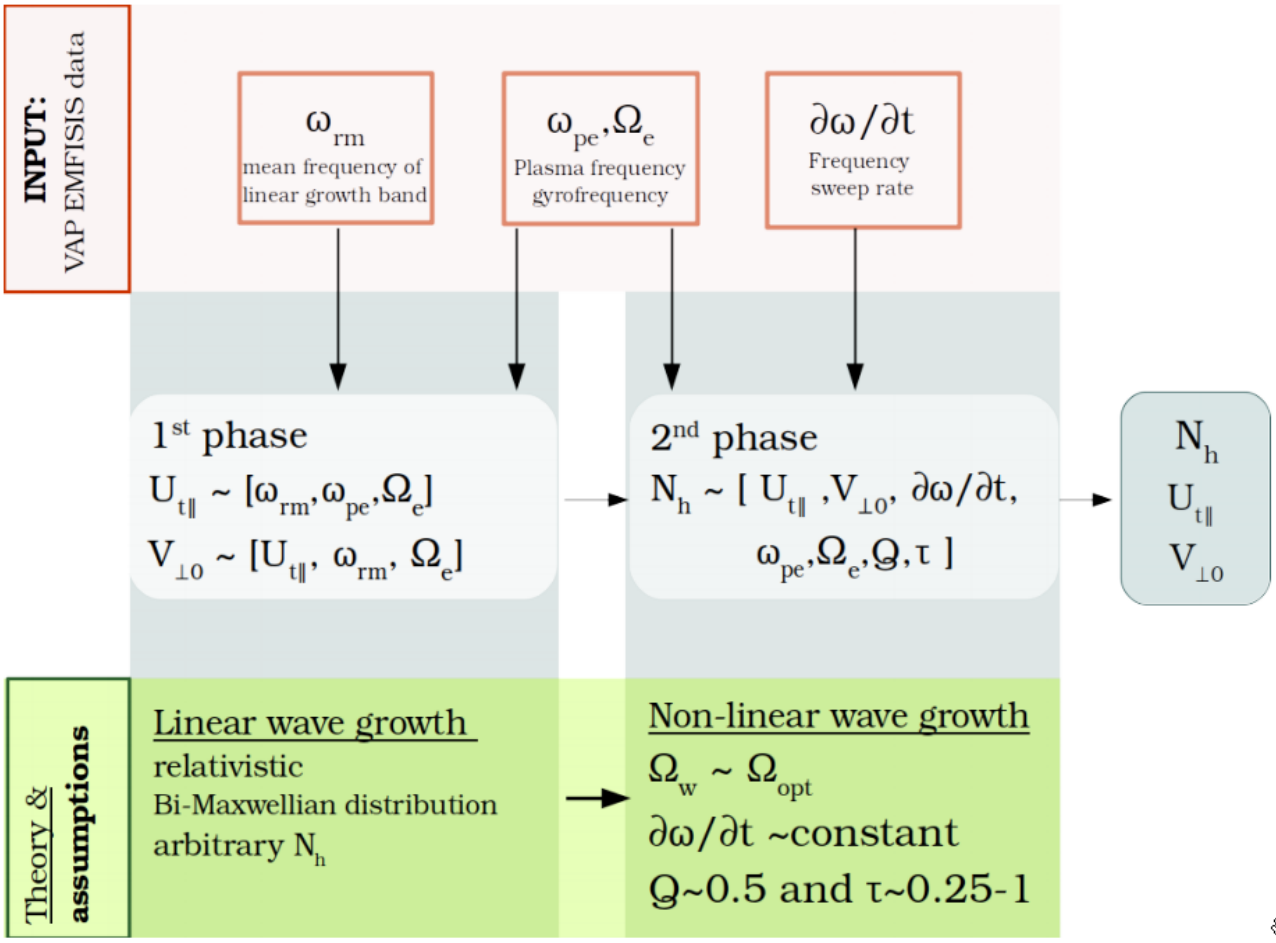

Figure 6. Chorus-inversion method: Inputs are from EMFISIS wave measurements (red boxes) only. As the first step, thermal momentum $U_{t||}$ and average perpendicular velocity $V_{\perp 0}$ are calculated assuming that linear wave growth is the initial phase of chorus generation. The second phase is governed by non-linear wave growth. Here, we replace the wave amplitude Ω_w with the optimum amplitude $\Omega_{opt}t$ in order to obtain N_h. For the calculation of N_h, we use the output of the first phase, $U_{t||}$ and $V_{\perp 0}$. At the end of the process, we obtain the bi-Maxwellian function parameters of energetic electrons responsible for chorus emission generation. In the green boxes we note some important assumptions.

The validation took place in two steps:

1. Validation of the inversion method using in-situ wave and particle measurements from Van Allen Probes.

The chorus waves were measured by the EMFISIS instrument (Figure 8.)

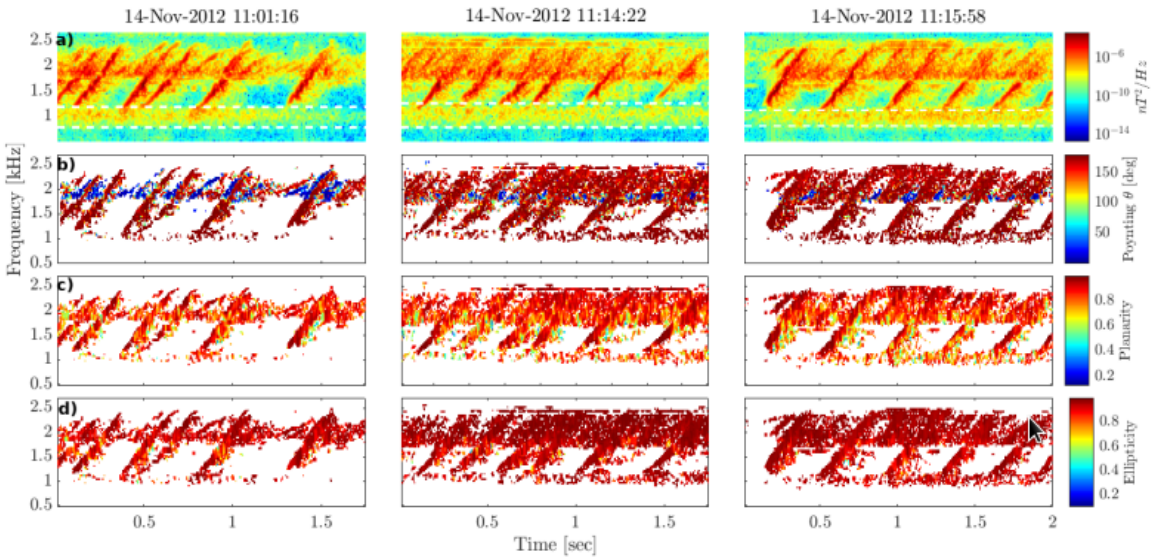

Figure 8. Van Allen Probes EMFISIS-A burst data recorded on 14 November 2012:11:01:16.67 UT (first column), 11:14:22.67 UT (second column), 11:15:58.67 UT (third column).a) Spectrogram of single-axis (BuBu) magnetic field. White dashed lines contour the assumed band of linear wave growth. b) Poynting vector angle θ with respect to the background geomagnetic field B0, c) Planarity and d) Ellipticity (magnetic PSD is greater than ~ $10^7 nT^2/Hz$)

The particle data were measured by HOPE instrument on Van Allen Probes, electron flux data is available as a function of energy and pitch angle. As we need compare the output of the inversion [N_h, $U_{t||}$, $V_{\perp 0}$], we derived the same quantities from HOPE measurements. Figure X+1 shows the results of the chorus inversion on a series of events.

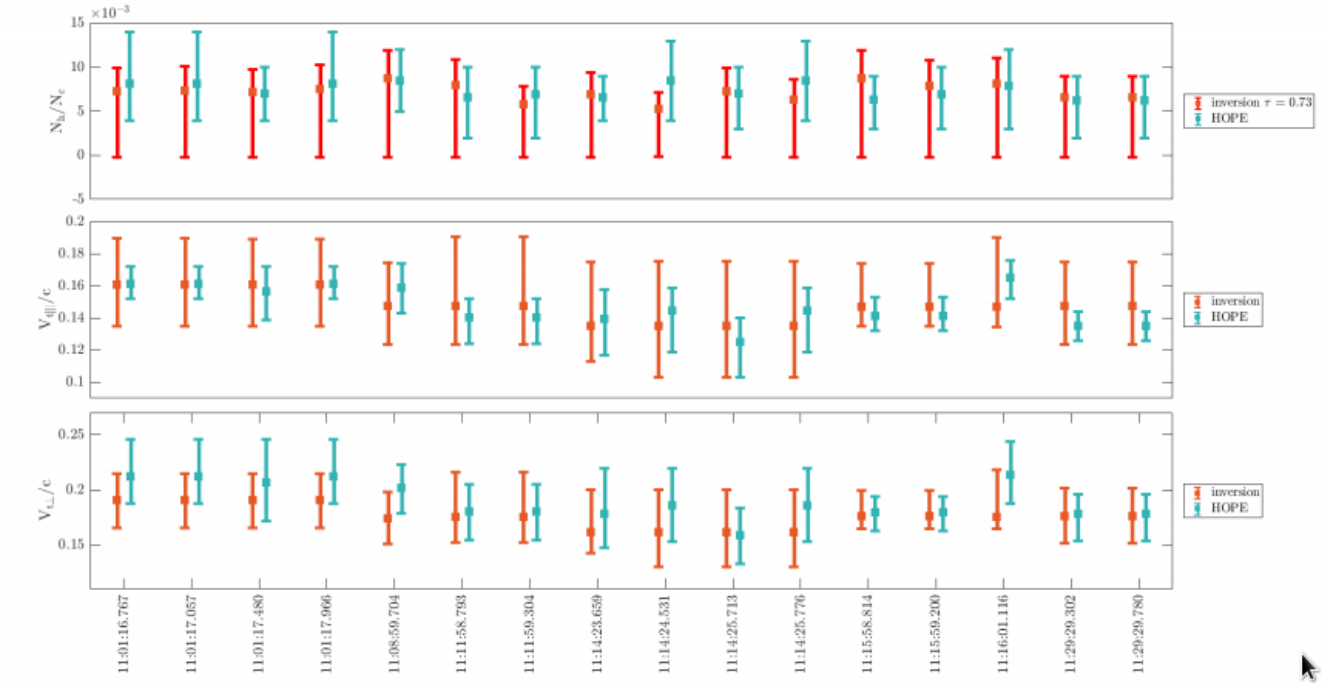

Figure 9. Results of the chorus-inversion of the selected 16 chorus emissions (referred by their date). N_h/N_c obtained from HOPE measurements are shown with blue error bars. The result of the inversion for N_h/N_c is a range (red errorbars), the minimum and maximum value of this interval corresponds to τ = 0.25 and 1, respectively. Top panel also shows the best fit of τ = 0.73 of the inversion to HOPE

measurements with red squares. Middle and bottom panel: parallel and perpendicular thermal velocities from the inversion (red) and HOPE (blue) with error bars.

2. Validation of the inversion method using ground based and ins-situ wave and in-situ particle measurements.

The ground based chorus waves were recorded at Halley, Antarctica (λ=-75.6 deg, φ=-26.6 deg, L=4.5), the particle data are form the HOPE instrument on Van Allen Probes.
For the validation based on ground based, simultaneous chorus events. This step is the most difficult one as satellite measurements are sporadic, both in time - we needed burst mode data from EMFISIS instrument, this measuring mode is rare due to the limited on board memory and telemetry capacity – and space – the satellite passes sporadically over the ground receiver location.
However, we found a simultaneous chorus event on 31 March 015 at 23:19:35 recorded by the EMFISIS instrument on Van Allen Probes (Figure 9) and 2 seconds later by AWDANet station Halley (Figure 10). First step of the validation was to remove the propagation effects using the chorus wave propagation model described in section T4 to obtain the dω/dt at the source region (magnetic equator). In the next step, the inversion was made using the in-situ and the 'backpropagated' ground chorus element and the results are compared with the energetic electron density N_h derived from in-situ HOPE particle measurements (Table 1).

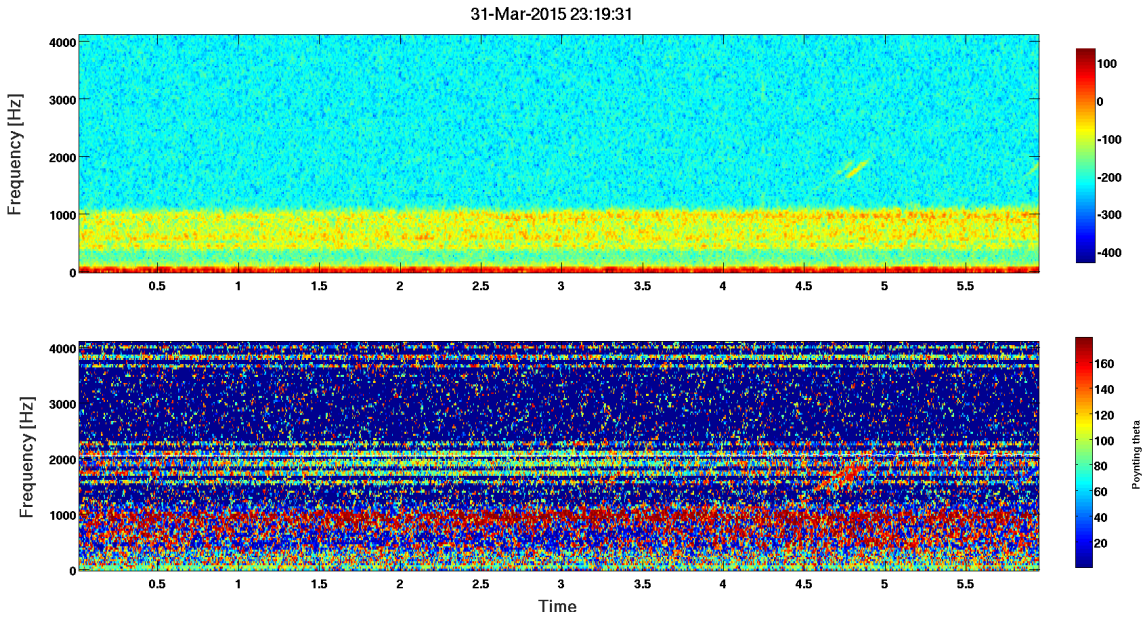

Figure 9. (top) Spectrogram of the chorus event recorded by the EMFISIS instrument at 23:19:34.5 on 31 March 2015, (bottom) angle between the background magnetic filed and the Poynting vector of the event.

The second step of the inversion validates the chorus wave propagation model also.

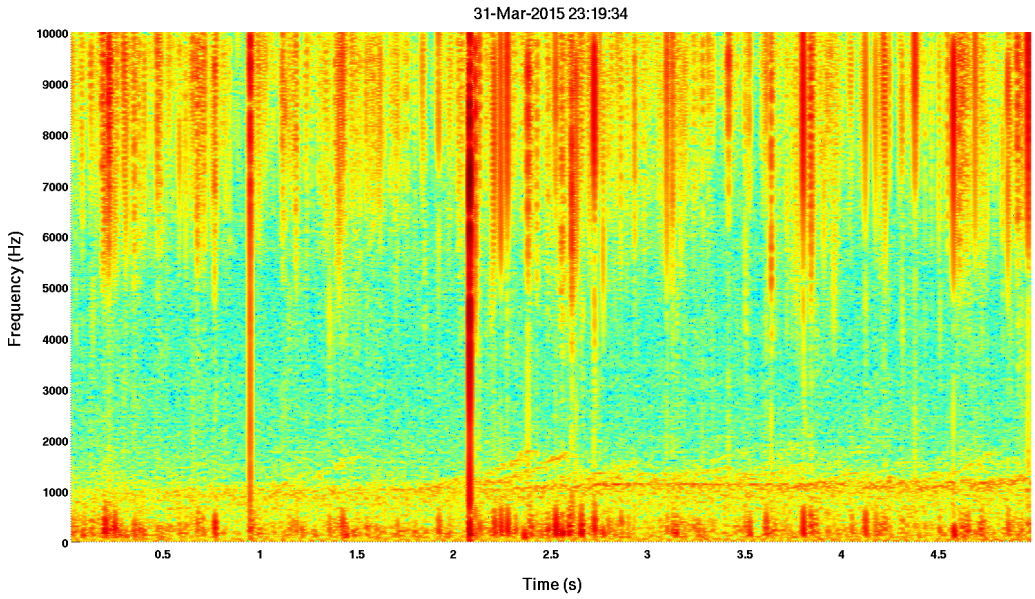

Figure 10. (top) Spectrogram of the simultaneous chorus event recorded by the AWDANet at Halley at 23:19:36.5 on 31 March 2015.

	HOPE particle data	EMFISIS chorus inversion	AWDANet chorus inversion
N_h/N_c, τ=1	0.0003+0.0001 -0.0002	0.0018+-0.0004	0.0013+0.0002 -0.0003
N_h/N_c, τ=0.25	0.0003+0.0001 -0.0002	0.0004+-0.0001	0.0003+0.0001 -0.0000

Table 1. The results of the validation on simultaneous chorus events. Note that the error on N_h/N_c is asymmetric (see details in Juhasz et al; , 2018).

Conclusions

We have successfully completed all the tasks in the workplan. The developed chorus inversion method has been validated by using both in-situ and ground based chorus measurements.

References

Berényi, K., V. Barta, Á. Kis (2017):Midlatitude ionospheric F2-layer response to eruptive solar events-caused geomagnetic disturbances over Hungary during the maximum of the solar cycle 24: A case study, Advances in Space Research, 61, 1230-1243, https://doi.org/10.1016/j.asr.2017.12.021

Carpenter, D. L. (1963), Whistler evidence of a 'knee' in the magnetospheric ionization density profile, *J. Geophys. Res.*, 68(6), 1675–1682.

Denton, R. E., J. D. Menietti, J. Goldstein, S. L. Young, and R. R. Anderson (2004), Electron density in the magnetosphere, J. Geophys. Res., 109, A09215, doi:10.1029/2003JA010245.

Ferencz Cs., Ferencz O.E., Hamar D. and Lichtenberger J. (2001): Whistler Phenomena, Short Impulse Propagation. Kluwer Academic Publisher, Netherlands, 1-260. ISBN 0-7923-6995-5

Golden, D. I., M. Spasojevic, F. R. Foust, N. G. Lehtinen, N. P. Meredith, and U. S. Inan (2010), Role of the plasmapause in dictating the ground accessibility of ELF/VLF chorus, J. Geophys. Res., 115, A11211, doi:10.1029/2010JA015955.

Helliwell, R. A. (1965). Whistlers and related ionospheric phenomena. Stanford: Stanford University Press.

Juhász L., J. Lichtenberger, Y. Omura , R. H. W. Friedel (2017): Inter-calibration of VAP-HOPE particle detectors to obtain the anisotropy of electron, 32nd URSI GASS, Montreal, 19-26 August 2017, https://ieeexplore.ieee.org/document/8104988

Juhász, Lilla, Yoshiharu Omura, János Lichtenberger, Reinhard H. Friedel (2018): Evaluation of plasma properties from chorus waves observed at the generation region, submitted to Journal of Geophysical Research: Space Physics, https://arxiv.org/abs/1811.09586

Kis, Arpad, Shuichi Matsukiyo, Fumiko Otsuka, Tohru Hada, Istvan Lemperger, Iannis Dandouras, Veronika Barta and Gabor Facsko, (2018): Effect of Upstream ULF Waves on the Energetic Ion Diffusion at the Earth's Foreshock. II. Observations, The Astrophysical Journal, 863:136, https://doi.org/10.3847/1538-4357/aad08c

Kis, Arpad, Lemperger Istvan, Voros Zoltan, Szalay Sandor and Shuichi Matsukiyo (2018): Scattering, injection and acceleration of field aligned beam ions at quasi-parallel shock: a hybrid simulation study, submitted to High Enegy Density Physics. ISSN 1574-1818, http://real.mtak.hu/id/eprint/88066

Koronczay, D., Lichtenberger, J., Juhász, L., Steinbach, P., & Hospodarsky, G. B. (2018). VLF transmitters as tools for monitoring the plasmasphere. Journal of Geophysical Research: Space Physics, 123. https://doi.org/10.1029/2018JA025802

Lichtenberger, J. (2009). A new whistler inversion method. Journal of Geophysical Research: Space Physics, 114 (A7).

Lichtenberger, J., Ferencz, C., Bodnár, L., Hamar, D., & Steinbach, P. (2008). Automatic whistler detector and analyzer system: Automatic whistler detector. Journal of Geophysical Research: Space Physics, 113 (A12).

Omura, Y., Katoh, Y., & Summers, D. (2008). Theory and simulation of the generation of whistler-mode chorus. Journal of Geophysical Research: Space Physics, 113 (A4).

Omura, Y., and Nunn, D. (2011). Triggering process of whistler mode chorus emissions in the magnetosphere. Journal of Geophysical Research: Space Physics,116 (A5).

Otsuka, Fumiko, Shuichi Matsukiyo, Arpad Kis, Kento Nakanishi and Tohru Hada (2018): Effect of Upstream ULF Waves on the Energetic Ion Diffusion at the Earth's Foreshock. I. Theory and Simulation, The Astrophysical Journal, 853:117, https://doi.org/10.3847/1538-4357/aaa23f

Xiao, F., Thorne, R. M., & Summers, D. (1998). Instability of electromagnetic rmode waves in a relativistic plasma. Physics of Plasmas, 5 (7), 2489-2497. DOI: 10.1063/1.872932

Zhelavskaya, I. S., M. Spasojevic, Y. Y. Shprits, and W. S. Kurth (2016), Automated determination of electron density from electric field measurements on the Van Allen Probes spacecraft, J. Geophys. Res. Space Physics, 121, 4611–4625, doi:10.1002/2015JA022132.